Available online at www.sciencedirect.com

ScienceDirect

Geochimica et Cosmochimica Acta 182 (2016) 24–39

Geochimica et Cosmochimica Acta

www.elsevier.com/locate/gca

Oxygen isotope analysis of fossil organic matter by secondary ion mass spectrometry

Romain Tartèse [a,b,*], Marc Chaussidon [c], Andrey Gurenko [d], Frédéric Delarue [a], François Robert [a]

[a] Institut de Minéralogie, de Physique des Matériaux et de Cosmochimie, Muséum National d'Histoire Naturelle, Sorbonne Universités, CNRS, UPMC & IRD, 75005 Paris, France

[b] Planetary and Space Sciences, The Open University, Walton Hall, Milton Keynes MK7 6AA, United Kingdom

[c] Institut de Physique du Globe de Paris (IPGP), CNRS UMR 7154, Université Sorbonne-Paris-Cité, Paris, France

[d] Centre de Recherches Pétrographiques et Géochimiques, UMR 7358, Université de Lorraine, 54501 Vandoeuvre-lès-Nancy, France

Received 15 September 2015; accepted in revised form 29 February 2016; available online 8 March 2016

Abstract

We have developed an analytical procedure for the measurement of oxygen isotope composition of fossil organic matter by secondary ion mass spectrometry (SIMS) at the sub-per mill level, with a spatial resolution of 20–30 μm. The oxygen isotope composition of coal and kerogen samples determined by SIMS are on average consistent with the bulk oxygen isotope compositions determined by temperature conversion elemental analysis – isotope ratio mass spectrometry (TC/EA-IRMS), but display large spreads of $\delta^{18}O$ of ~5–10‰, attributed to mixing of remnants of organic compounds with distinct $\delta^{18}O$ signatures. Most of the $\delta^{18}O$ values obtained on two kerogen residues extracted from the Eocene Clarno and Early Devonian Rhynie continental chert samples and on two immature coal samples range between ~10‰ and ~25‰. Based on the average $\delta^{18}O$ values of these samples, and on the O isotope composition of water processed by plants that now constitute the Eocene Clarno kerogen, we estimated $\delta^{18}O_{water}$ values ranging between around −11‰ and −1‰, which overall correspond well within the range of O isotope compositions for present-day continental waters. SIMS analyses of cyanobacteria-derived organic matter from the Silurian Zdanow chert sample yielded $\delta^{18}O$ values in the range 12–20‰. Based on the O isotope composition measured on recent cyanobacteria from the hypersaline Lake Natron (Tanzania), and on the O isotope composition of the lake waters in which they lived, we propose that $\delta^{18}O$ values of cyanobacteria remnants are enriched by about ~18 ± 2‰ to 22 ± 2‰ relative to coeval waters. This relationship suggests that deep ocean waters in which the Zdanow cyanobacteria lived during Early Silurian times were characterised by $\delta^{18}O$ values of around −5 ± 4‰. This study, establishing the feasibility of micro-analysis of Phanerozoic fossil organic matter samples by SIMS, opens the way for future investigations of kerogens preserved in Archean cherts and of the O isotopic composition of ocean water at that period in time.

1. INTRODUCTION

The temperature of Archean oceans has been a topic of great controversies for half a century since the recognition that the oxygen isotope composition of sedimentary cherts, expressed using the $\delta^{18}O$ notation ($\delta^{18}O = [^{18}O/^{16}O_{sample}/^{18}O/^{16}O_{SMOW} - 1] \times 1000$, where SMOW is the Standard Mean Ocean Water), increased by about

* Corresponding author at: Institut de Minéralogie, de Physique des Matériaux et de Cosmochimie, Muséum National d'Histoire Naturelle, Sorbonne Universités, CNRS, UPMC & IRD, 75005 Paris, France.

E-mail address: romain.tartese@mnhn.fr (R. Tartèse).

http://dx.doi.org/10.1016/j.gca.2016.02.035

0016-7037/

15–20‰ from ~3.5 billion-year ago to the present-day (Perry, 1967; Knauth and Epstein, 1976; Knauth and Lowe, 1978). The oxygen isotopic composition of silica precipitated from a fluid is related to the isotopic composition of the fluid and to the temperature T at which precipitation occurred, according to the equation: $1000 \times \ln(\Delta^{18}O) = (3.09 \times 10^6 \times T^{-2}) - 3.29$ (Knauth and Epstein, 1976), where $\Delta^{18}O = \delta^{18}O_{chert} - \delta^{18}O_{water}$. This equation contains three variables: the temperature T of the fluid from which cherts precipitated, $\delta^{18}O_{water}$ and $\delta^{18}O_{chert}$. Therefore, it is not possible to derive both the temperature and the isotopic composition of seawater based on measurements of $\delta^{18}O_{chert}$ without making an assumption on either the seawater T or its O isotope composition. As a result, and considering only Precambrian cherts with pristine O isotope composition not modified during secondary alteration (see for example the recent reviews by Perry and Lefticariu, 2014), two end-member scenarios (not mutually exclusive) have been proposed to explain the observed secular trend of the chert $\delta^{18}O$ values:

(1) Archean oceans were characterised by temperatures up to around 50–70 °C higher than today, which implies that the O isotope composition of oceanic waters has remained globally constant around 0‰ throughout the Earth history (Knauth and Epstein, 1976; Knauth and Lowe, 1978, 2003; Knauth, 2005). This scenario is supported by other proxies, such as Si isotopes in cherts, which show variations consistent with a ~50 °C decrease in temperature from the early Archean (e.g., Robert and Chaussidon, 2006), or O isotope composition of serpentine in ophiolite rocks, and notably from those of the *ca.* 3.8 Ga Isua Supracrustal Belt (e.g., Pope et al., 2012).
(2) Archean oceans were characterised by $\delta^{18}O$ values lower by about 10–15‰ compared to present day, in which case surface temperatures on the Earth have remained globally constant since ~3.5 Ga (e.g., Kasting et al., 2006; Jaffrés et al., 2007; Hren et al., 2009). This scenario is consistent with the proposed existence of major Archean and Proterozoic glaciations (e.g., Evans et al., 1997; Young et al., 1998), suggesting that surface conditions on the Earth were not drastically different to today during the Precambrian. This scenario is also in line with the lack of evidence for a high atmospheric pressure of CO_2 in Archean sediments that would have been required to maintain high surface temperature under a Sun much fainter than today (e.g., Lowe and Tice, 2004; Kasting et al., 2006; Jaffrés et al., 2007), even though recent modelling studies have suggested that fewer amounts of greenhouse gases (CO_2 and CH_4) are in fact required to counteract the "faint young Sun problem" (Charnay et al., 2013).

Recent *in situ* studies of the O and Si isotope composition variations at the micrometre scale in cherts have shown that transformation of amorphous silica precursors during diagenesis is accompanied by isotopic fractionation in micrometre-scale domains (Marin et al., 2010; Marin-Carbonne et al., 2012). For the *ca.* 1.9 Ga Gunflint chert for example, this observation implies a lowering by ~20 °C of the seawater temperature (~37–52 °C) calculated from $\delta^{18}O_{chert}$, which, however, remains much higher than present day temperature (Marin et al., 2010; Marin-Carbonne et al., 2012).

These two end-member scenarios have fundamental implications, notably for understanding the early-Earth environmental conditions that promoted the appearance and evolution of life *ca.* 3.4–3.5 Gyr ago (e.g., Schopf, 1993; Tice and Lowe, 2004; Wacey et al., 2011; Brasier et al., 2015). Putative and *bona fide* early-life remnants, found as micrometre-size insoluble organic matter (OM) patches disseminated in cherts (e.g., Schopf, 1993; Tice and Lowe, 2004; Wacey et al., 2011; Brasier et al., 2015), can potentially provide us with an independent way of constraining the O isotope composition of Archean seawater. Indeed, the O isotope composition of organic compounds, such as cellulose or lipids, is thought to be primarily controlled by the isotopic composition of the water in which they formed, but seems to be relatively insensitive to the temperature of this water (e.g., DeNiro and Epstein, 1981; Sternberg and DeNiro, 1983; Silva et al., 2015). While the study of the C and S isotope characteristics of carbonaceous OM patches and associated sulphides, notably through *in situ* ion microprobe studies, has been used to argue for their biological origin and to show that they can preserve isotopic information throughout geological times (e.g., House et al., 2000; Ueno et al., 2001; Wacey et al., 2011; Bontognali et al., 2012; Williford et al., 2013; Fischer et al., 2014), their O isotope composition has never been investigated.

Here we present a detailed analytical approach establishing the feasibility of analysing the O isotope composition of fossil OM by secondary ion mass spectrometry (SIMS) on well characterised Phanerozoic samples, including the characterisation of a kerogen sample that can be used as a SIMS reference material for O isotope analysis. Carbonaceous remnants have low O abundances (~5–15 wt.%; e.g., Durand and Monin, 1980) and typically occur as small micrometre-scale patches disseminated in a O-rich quartz matrix. Therefore, analyses were carried out on insoluble OM residues isolated from the chert samples by acid digestion. However, extracted residues are not pure OM and contain many O-bearing micro-inclusions of diverse mineral phases. Our analytical approach thus includes a procedure allowing for filtering the O isotope data compromised by analysis of mineral micro-inclusions, based on measurements of the intensities of species such as ^{28}Si, ^{32}S and $^{56}Fe^{16}O$. We have applied this approach to five coal and kerogen samples ranging in age from Eocene to Silurian and on recent chert-hosted cyanobacteria remnants. Based on these results obtained on Phanerozoic samples, we have investigated (i) how does fossil OM preserve its O isotope signature, (ii) what is the bulk oxygen isotope fractionation between OM and water, and (iii) what are the potential implications for deriving the O isotope composition of paleo-waters from that of coeval OM. These results will be crucial for future studies applying

a similar approach to kerogen residues extracted from cherts as old as ~3.5 Ga in order to reconstruct the O isotopic composition of Archean oceans. Ultimately, combining these independent constraints on the O isotopic composition of oceanic waters through time with the secular chert O isotope record should allow reconstructing the temperature variations of the oceans throughout the Earth history.

2. STUDIED SAMPLES

We have investigated two coal samples, Blind Canyon and Illinois #6, which are both part of the Argonne Premium Coal Sample Program (Vorres, 1990), three kerogen samples that were extracted from the Eocene chert Clarno (USA), from the Early Devonian chert Rhynie (Scotland) and from the Silurian chert Zdanow (Poland), respectively, and the acid-resistant OM fraction extracted from ~10 kyr old cherts formed in the hypersaline Lake Natron (Tanzania) (Table 1). These samples cover a large range of ages and conditions of formation. For some of them, the O isotopic composition of the water associated with the organic matter is known, allowing to investigate O isotope fractionation between organic matter and the water associated with it.

The kerogen samples were isolated from the cherts using HF/HCl acid maceration (Durand and Nicaise, 1980). Throughout the whole isolation procedure the use of paper fibre was excluded to avoid any potential contamination. The chert samples were crushed in a mechanical crusher, which was previously cleaned using ethanol. The soluble compounds were extracted with an Accelerated Solvent Extractor (ASE) using a dichloromethane/methanol (2/1: v/v) solvent mixture in order to minimise post-deposition contamination. The remaining powder was submitted to a first acidic treatment using HCl 6 N and then to a second acidic treatment using a HF (40%)/HCl 6 N (2/1: v/v) mixture at room temperature. A final acidic treatment was conducted, using HCl 6 N at 60 °C, to dissolve any fluorides that may have been formed during the previous acidic treatments. This HF/HCl protocol systematically involved rinsing and centrifugation between each extraction step in order to avoid pollution by the released dissolved organic compounds. The extracted kerogens were investigated through Raman micro-spectroscopy, which yielded spectra typical of those found in kerogens that have suffered thermal alteration, ensuring that they have not been affected by laboratory contamination (Bourbin, 2012).

2.1. Natron OM

Organic matter was extracted from a chert sample collected in 2012 about 50 m above the present-day shoreline of the Lake Natron in Tanzania (GPS coordinates 2°22′43″S, 35°54′24.00″E), which likely formed during the last maximum lacustrine extension in the Lake Natron-Lake Magadi area about 10 kyr ago (Hillaire-Marcel et al., 1986; Hillaire-Marcel and Casanova, 1987). Several mechanisms have been suggested to explain chert formation in the Natron-Magadi area. Eugster (1967, 1969) proposed that formation of the bedded chert horizons resulted from leaching of Na from previously deposited magadiite ($NaSi_7O_{13}(OH)_3 \cdot 3H_2O$) and kenyaite ($NaSi_{11}O_{20.5}(OH)_4 \cdot 3H_2O$) layers by percolating ground waters. Hay (1968) and O'Neil and Hay (1973) also argued for formation of the cherts from Na-silicate precursors due to interaction with waters of varying salinity, from dilute meteoric water to highly saline lake water. On the other hand, Behr and Röhricht (2000) published the first description of diverse microbial communities in Magadi-type cherts, such as cyanobacteria (i.e. *Pleurocapsa* sp. and *Gloeocapsa* sp.), and argued that Magadi-type cherts formed predominantly by silicification of calcified cyanobacterial mats and bioherms in shallow lake waters and for an organic origin for most of the chert horizons in the Natron-Magadi area. Additionally, samples of today's Lake Natron waters were also collected by A. Person in 2012 and their O isotope compositions were analysed at ECOLAB, Laboratoire d'écologie fonctionnelle (UMR 5245, Toulouse, France).

2.2. Blind Canyon coal

The Early-Campanian Blind Canyon coal sample is a high-volatile bituminous coal and was collected in Emery County, Utah, in the Upper Cretaceous Blackhawk Formation from the Mesaverde Group (Pierce et al., 1989; Vorres, 1990). Sedimentary units in the Blackhawk Formation comprise channel sandstones interbedded with mudstones

Table 1
Main geological characteristics of the studied samples.

Sample	Type	Age (Ma)	Location	References
Natron	Organic matter	~0.010	Lake Natron, Tanzania	Eugster (1969) and Hillaire-Marcel et al. (1986)
Clarno	Kerogen	40	Clarno Formation, John Day Basin, Oregon, USA	Schopf et al. (1983) and Czaja et al. (2009)
Blind Canyon	Coal	80	Blackhawk Formation, Mesaverde Group, Utah, USA	Pierce et al. (1989) and Vorres (1990)
Illinois #6	Coal	~310	Herrin seam, Carbondale Formation, Illinois, USA	Willman et al. (1975) and Vorres (1990)
Rhynie	Kerogen	410	Rhynie, Dryden Flags Formation, Aberdeenshire, Scotland	Rice et al. (1995, 2002) and Mark et al. (2011)
Zdanow	Kerogen	440	Zdanow, Bardzkie Mountains, Sudetes Mountains, Poland	Kremer and Kaźmierczak (2005)

and siltstones deposited in a deltaic environment, where extensive swamps developed from which the large and continuous coal beds were derived (Pierce et al., 1989). The Blind Canyon coal is immature, with a vitrinite reflectance R_o of *ca.* 0.5% (Cloutis, 2003), and contains high liptinite abundances, indicating that the vegetation that comprised the OM of the Blind Canyon swamp must have been very resinuous (Pierce et al., 1989). In addition, Parker (1976) proposed that the dominant flora included evergreen conifers and angiosperms that developed in a shallow water environment in a warm-temperate to subtropical climate.

2.3. Illinois #6 coal

The Illinois #6 coal sample is a high-volatile bituminous coal and was collected from the Herrin seam, ~100 km southeast of St. Louis, Illinois, in the Pensylvanian Carbondale Formation (Vorres, 1990). The Carbondale Formation contains grey silty shales and sandstones, often appearing as elongated thick channels, formed in flood plains and deltaic environments, and in which swamps developed and resulted in the formation of the various coal beds of the Carbondale Formation, including the Illinois #6 coal bed (Willman et al., 1975). The Carbondale Formation also comprises dark-grey to black shales and grey limestones containing remnants of marine fossils deposited in shallow seas (Willman et al., 1975). The Illinois #6 coal is immature, with a vitrinite reflectance R_o of *ca.* 0.5% (Cloutis, 2003). Arborescent lycopods were the major constituents of the biomass of the Illinois #6 swamps, which also comprised ferns and pteridosperms, indicating wetlands surrounded by forest environments with standing water (DiMichele and Phillips, 1988).

2.4. Clarno kerogen

The Clarno chert (sample PPRG 456) was collected in the John Day basin in the Late Eocene, ~40 Myr old, Clarno Formation in Oregon, USA (Schopf et al., 1983; Walter et al., 1983). This black carbonaceous chert is interpreted to have formed in a marsh environment, in which silica was derived from nearby hot springs, evaporation and overburden pressure resulting in lithification of the bedded chert and permineralisation of the fossil plants (e.g., Arnold and Daugherty, 1964). Fossil floras of the Clarno chert have been extensively studied and comprise mm- to cm-size specimens typical of marsh plants such as ferns, bryophytes and aquatic angiosperms together with fruits and seeds deposited from local terrains (e.g., Czaja et al., 2009; Shi et al., 2013).

2.5. Rhynie kerogen

The Rhynie chert site is one of the earliest known subaerial hot spring systems, the chert horizons being part of Early Devonian sedimentary and volcanic units dated around 400–410 Ma (e.g., Rice et al., 1995; Mark et al., 2011). At that time, hot spring activity led to the formation of siliceous sinters that ensured unique preservation of the flora and fauna, comprising early vascular land plants, lichens, fungi, algae, terrestrial arachnids and insects and freshwater crustaceans (e.g., Rice et al., 2002, and references therein). In the studied sample, microscopic observations revealed the presence of numerous spherical microfossils (spores, sporocysts, cyanobacteria, algae) and of long woody remnants hosted within a micro-crystalline silica matrix (Bourbin, 2012). The Rhynie chert horizons are hosted by lacustrine shales and muddy sandstones of the Dryden Flags Formation that corresponded to a low energy fluvio-lacustrine environment (Rice et al., 2002). The cherts themselves probably formed in freshwater pools in the vicinity of Si-rich hot spring vents (Rice et al., 2002).

2.6. Zdanow kerogen

The Zdanow chert was collected near the Żdanów village in the Bardzkie Mountains, Sudetes, in southwestern Poland, from a layer of black radiolarian chert intercalated with black siliceous chert layers (Kremer and Kaźmierczak, 2005; Kremer, 2006). The ~5–10 cm thick beds of black radiolarian cherts are composed of fine crystalline chalcedony. In the cherts, degraded benthic coccoid cyanobacterial mats are observed as laminated OM horizons, while remains of cyanobacteria also occur as agglomerations of subglobular colonies (Kremer and Kaźmierczak, 2005; Kremer, 2006). Their structural and morphological characteristics permit to compare this Silurian microbiota to some modern unicellular coccoid cyanobacteria (Kremer and Kaźmierczak, 2005; Kremer, 2006). According to Kremer (2006), the lithological context and palaeogeographical position of these early Silurian mats indicate that these cyanobacteria lived in relatively deep and weakly illuminated marine environments.

3. ANALYTICAL APPROACH

Direct *in situ* O isotope analysis of OM in chert samples using any microbeam technique is very challenging, because of the small size of the organic fragments and the potential strong contamination by oxygen from surrounding quartz. Thus, OM must be extracted from the chert samples. After isolation, the coal and kerogen samples were grinded into a fine powder, from which a few mg were pressed into high purity indium (99.999%) and then carbon coated for further investigation using secondary electron microscopy (SEM) and SIMS.

3.1. Anticipated hurdles related to O isotope analysis of OM at the micrometre scale by SIMS

Despite the potential of SIMS to allow O isotope analysis of OM, several important issues can be anticipated, probably explaining why such type of analysis has never been developed before:

- Oxygen abundance in fossil OM (coal, kerogen) is low, typically between around ~3 and 25 wt.%, with an average around 10 wt.% (e.g., Durand and Monin, 1980; Vorres, 1990).

- Fossil OM contains micro-inclusions of O-rich mineral phases such as oxides, even after isolation of the kerogen residues following the HF-HCl treatment. Because the ion emissivity of O from Ti- or Fe-oxide is strong relative to that from OM (see Section 5.1), and because these oxides contain elevated O contents, the secondary O signal emitted from a mix of OM and oxides can be strongly influenced, and even dominated, by that from oxides.
- Reference material with established $^{18}O/^{16}O$ ratios does not exist for correction of instrumental mass fractionation (IMF) produced during SIMS analysis of O isotopes.

To overcome these potential issues, we have investigated two coal samples, three kerogen samples and one recent OM sample also isolated by acid treatment, combining bulk O isotope analysis and ion microprobe analysis. We have also investigated the mineralogy of the kerogen samples using secondary electron microscopy to track the effects of contamination of the spot area by mineral inclusions.

3.2. Bulk O isotope analysis

Bulk O isotope compositions were determined by TC/EA-IRMS at Iso-Analytical Ltd. (Cheshire, UK) on four selected samples (Table 2). Silver capsules were loaded with 3 mg of sample, sealed and oven-dried at 60 °C for 10 days prior to analysis to remove moisture. The O isotope analyses were conducted by total conversion at 1080 °C in a quartz reactor tube lined with a glassy carbon film, filled to a height of 170 mm with glassy carbon chips and topped with a layer of 50% nickelised carbon (10 mm deep). Carbon monoxide (CO) and nitrogen (N) produced were separated on a GC column packed with a molecular sieve 5A (1 m long ANCA-SL/GSL from Elemental Microanalysis, UK) at a temperature of 65 °C. CO composition was measured by IRMS using a Europa Scientific 20–20 instrument equipped with a triple Faraday cup collector array. Samples were measured together with the reference material IAEA-CH-6 (sucrose, 51.4 wt.% O and $\delta^{18}O = 36.4‰$), which was also used to calibrate the amount of O extracted from the samples. IAEA-CH-3 (cellulose, $\delta^{18}O = 32.2‰$) and FIRMS 221-1 (nylon, $\delta^{18}O = 10.3‰$) were run for quality control, and yielded $\delta^{18}O$ values of $31.8 \pm 0.1‰$ ($n = 2$) and $10.7 \pm 0.1‰$ ($n = 2$), respectively. All the bulk data reported in this study (Table 2) are given at the 2σ level and include variability associated with repeated analyses of individual samples and the reproducibility measured on the reference sucrose sample.

3.3. SIMS O isotope analyses

Microanalysis of O isotope compositions was carried out at the Centre de Recherches Pétrographiques et Géochimiques (CRPG) in Nancy (France) during two analytical sessions, using the Cameca IMS 1280 HR ion probe in February 2015 and the Cameca IMS 1270 E7 ion probe in July 2015. The analytical protocols were identical for both instruments during these two analytical sessions. Isotopes of ^{16}O and ^{18}O were first analysed using a Cs^+ primary beam of ~10 nA with an acceleration voltage of 10 kV rastered over 20–30 μm diameter areas, using the electron gun for charge compensation. Secondary ions were accelerated at 10 kV and measured in multicollection mode using two Faraday cups (FC) on the L'2 trolley for ^{16}O and on the H1 trolley for ^{18}O with a mass resolving power set to ~2500 (using slit #1 in multicollection mode), sufficient to resolve $^{18}O^-$ from the interfering $^1H_2{}^{16}O^-$ species. For each analysis, the FC backgrounds were measured during pre-sputtering, and the measured $^{18}O/^{16}O$ ratios were corrected for background using the average of background measurements performed immediately before (during pre-sputtering of analysis n) and immediately after (during pre-sputtering of analysis $n + 1$). The total analytical time for O isotope analysis was ~5–6 min, including pre-sputtering (60 s) and counting the secondary oxygen ions during 50–60 cycles each of 5 s. Also, the secondary species $^{12}C^1H$, ^{16}O, ^{28}Si, ^{32}S and $^{56}Fe^{16}O$ were then collected in the axial FC at a mass resolving of ~4000 during a separate acquisition, using the magnetic peak switching mode on the same analytical spots and a ~1–10 nA Cs^+ beam, depending on C and O intensities, in order to identify contamination of OM by residual silica, sulphides, Fe-chromite or Fe-oxides. Therefore, it should be pointed out that the volume of materials sampled during both sequences of analyses are different and that nugget effects resulting from ablating mineral micro-inclusions cannot be entirely ruled out as a potential cause of some of the heterogeneity of the O isotope composition reported for OM.

All measurements of ^{18}O, whatever the intensity, were carried out on a FC, thus not using an electron multiplier

Table 2
Elemental and isotopic composition measured on the coal and kerogen samples.

Sample	Type	Elemental composition[a] (wt.%)					Atomic ratio		Isotopic composition	
		C	H	N	O	$O_{EA\text{-}IRMS}$[b]	H/C	O/C	$\delta^{18}O_{bulk}$ (‰)	$\delta^{18}O_{SIMS}$ (‰)
Blind Canyon	Coal	80.7	5.8	1.6	11.6	13.9	0.86	0.13	12.7 ± 0.4	8.7 ± 3.6
Illinois #6	Coal	77.7	5.0	1.4	13.5	16.1	0.77	0.16	13.5 ± 0.2	16.6 ± 2.6
Clarno	Kerogen	44.8	2.8	*nd*	*nd*	24.3	0.75	0.41	14.3 ± 0.1	13.9 ± 0.5
Rhynie	Kerogen	31.3	2.1	*nd*	*nd*	*nd*	0.81	–	*nd*	19.0 ± 2.1
Zdanow	Kerogen	69.4	2.6	*nd*	*nd*	21.2	0.45	0.23	13.4 ± 0.2	15.3 ± 1.2

nd: not determined.
[a] Moisture and ash-free compositions after Vorres (1990) for the coal samples and Bourbin (2012) for the kerogen samples.
[b] O abundances determined by TC/EA-IRMS (this study).

(EM) for low ^{18}O counts rates. This approach was chosen to avoid additional uncertainties related to the inter-calibration between the gains of the FC and the EM, and to the drift of the EM efficiency with time. Due to the low abundance of O in some of the studied coal and kerogen samples, the ^{18}O intensities measured on the H1 FC were often low, between $\sim 1 \times 10^5$ and $\sim 1 \times 10^6$ cps. Therefore, we tested the linearity of the H1 FC for variable ^{18}O intensities by carrying out repeated analysis of the CRPG reference quartz NL615 ($\delta^{18}O_{SMOW} = 18.4‰$) while varying the primary Cs^+ beam intensity between ~50 pA and ~5 nA. The raw $\delta^{18}O$ values (not corrected for IMF) measured for different primary beam intensities during two analytical sessions in January and February 2015 display an increase of the dispersion of the values around the average $\delta^{18}O$ with decreasing ^{18}O intensity, but globally $\delta^{18}O$ values measured over a range of ^{18}O intensities from $\sim 2 \times 10^5$ to $\sim 9 \times 10^6$ cps are consistent for each analytical session, averaging $12.6 \pm 0.3‰$ (2SE, $n = 4$) and $10.1 \pm 0.4‰$ (2SE, $n = 5$) for the January and February 2015 sessions, respectively (Fig. 1). In addition, note that changing the primary intensity by about two orders of magnitude could have induced slight variations of instrumental mass fractionation of O isotopes, which are likely partly the cause of the 0.3–0.4‰ variations observed for the averaged measured $\delta^{18}O$ values. Therefore, these tests show that the low ^{18}O intensities inherent to measurements of coal and kerogen samples, all carried out using a 5–10 nA primary beam current, did not cause significant shifts of the $^{18}O/^{16}O$ ratios.

The uncertainties associated with the SIMS $\delta^{18}O$ values must include uncertainties related to (i) the counting statistics associated with each individual analysis, (ii) the external reproducibility measured on a homogeneous standard, and (iii) the uncertainty on the bulk 'true' $\delta^{18}O$ for the standard determined by TC/EA-IRMS. As discussed below, the Clarno kerogen sample was found to be the most homogeneous and was used to estimate both the typical external reproducibility and the uncertainty on IMF. Uncertainties

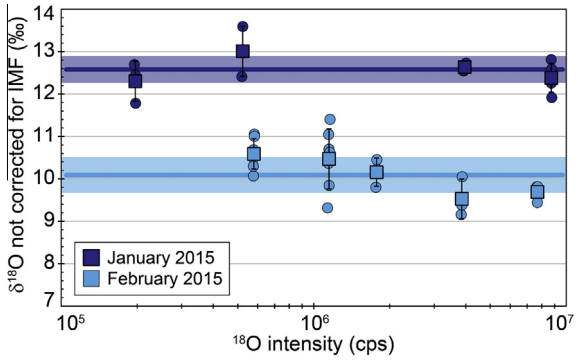

Fig. 1. Oxygen isotope composition measured on the CRPG reference quartz NL615 for various primary beam currents, represented here as variable ^{18}O intensities. The $\delta^{18}O$ values are not corrected for instrumental mass fractionation (IMF), which changed slightly by ~2.5‰ between the two sessions. No significant shift of $\delta^{18}O$ values is observed over a two orders of magnitude change of ^{18}O intensity.

reported in Table 2 for SIMS $\delta^{18}O_{SMOW}$ values include all the sources of errors mentioned above and are given at the 2σ level.

3.4. Secondary electron microscopy

The analytical pits produced during O isotope analyses were examined in details in selected samples in order to check for the presence of mineral impurities (silica, sulphides, chromites, Fe-oxides) embedded within OM using a TESCAN VEGA II SEM at the MNHN in Paris (France) operated with a 15 kV voltage. Mineral impurities were located on back-scattered electron (BSE) images and qualitatively analysed using Energy Dispersive X-ray Spectroscopy (EDS).

4. RESULTS

4.1. Bulk O isotopes

Analyses of the Blind Canyon and Illinois #6 coal samples yielded bulk O abundances of 13.9 ± 2.7 wt.% (2SE, $n = 4$) and 16.1 ± 2.9 wt.% (2SE, $n = 4$), respectively, which is slightly higher than the O contents of ~11.6 wt.% and 13.5 wt.% (moisture and ash-free basis) determined on the same samples by Vorres (1990) (Table 2). Although there is no definitive way to accurately measure the O yield of the TC/EA-IRMS bulk analyses, the consistency of our results with those obtained by Vorres (1990) suggests that our bulk O abundances are accurate. In addition, the sum of the literature C + H + N and of our TC/EA-IRMS O abundance yields 102.0 wt.% and 100.2 wt.% for Blind Canyon and Illinois #6 coal samples, respectively, suggesting that these elemental compositions are accurate at a few percent level. Analyses of Clarno and Zdanow kerogens yielded 24.3 ± 2.7 wt.% O ($n = 2$) and 21.2 ± 2.7 wt.% O ($n = 2$), respectively. The Blind Canyon and Illinois #6 coal samples yielded $\delta^{18}O$ values of $12.7 \pm 0.4‰$ (2SE, $n = 4$) and $13.5 \pm 0.2‰$ (2SE, $n = 4$), respectively (Table 2). The bulk oxygen isotope compositions of the kerogen samples are similar, with $\delta^{18}O$ values of $14.3 \pm 0.1‰$ ($n = 2$) and $13.4 \pm 0.2‰$ ($n = 2$) for Clarno and Zdanow, respectively (Table 2).

4.2. SIMS analyses: O isotopes and elemental contents

All the $\delta^{18}O$ values measured for the six samples are displayed in Fig. 2 (each dot corresponding to a different spot of analysis), together with the corresponding $^{12}C^1H$, ^{16}O, ^{28}Si, and $^{56}Fe^{16}O$ intensities (normalised to the primary beam intensity). All the data are provided in the Supplementary Table 1. For the kerogen and Natron OM samples, the $\delta^{18}O$ values vary by about 8–12‰, while they vary by up to ~34‰ and ~40‰ for the Blind Canyon and Illinois #6 coal samples, respectively (Fig. 2). The measured $\delta^{18}O$ values cluster around −15‰ for the Clarno and Zdanow kerogens, and around $-10 \pm 5‰$ and $0 \pm 5‰$ for the Rhynie kerogen and Natron OM, respectively (Fig. 2).

Large variations are observed at the spot scale in a given sample for $^{12}C^1H$, ^{16}O, ^{28}Si, ^{32}S and $^{56}Fe^{16}O$ intensities

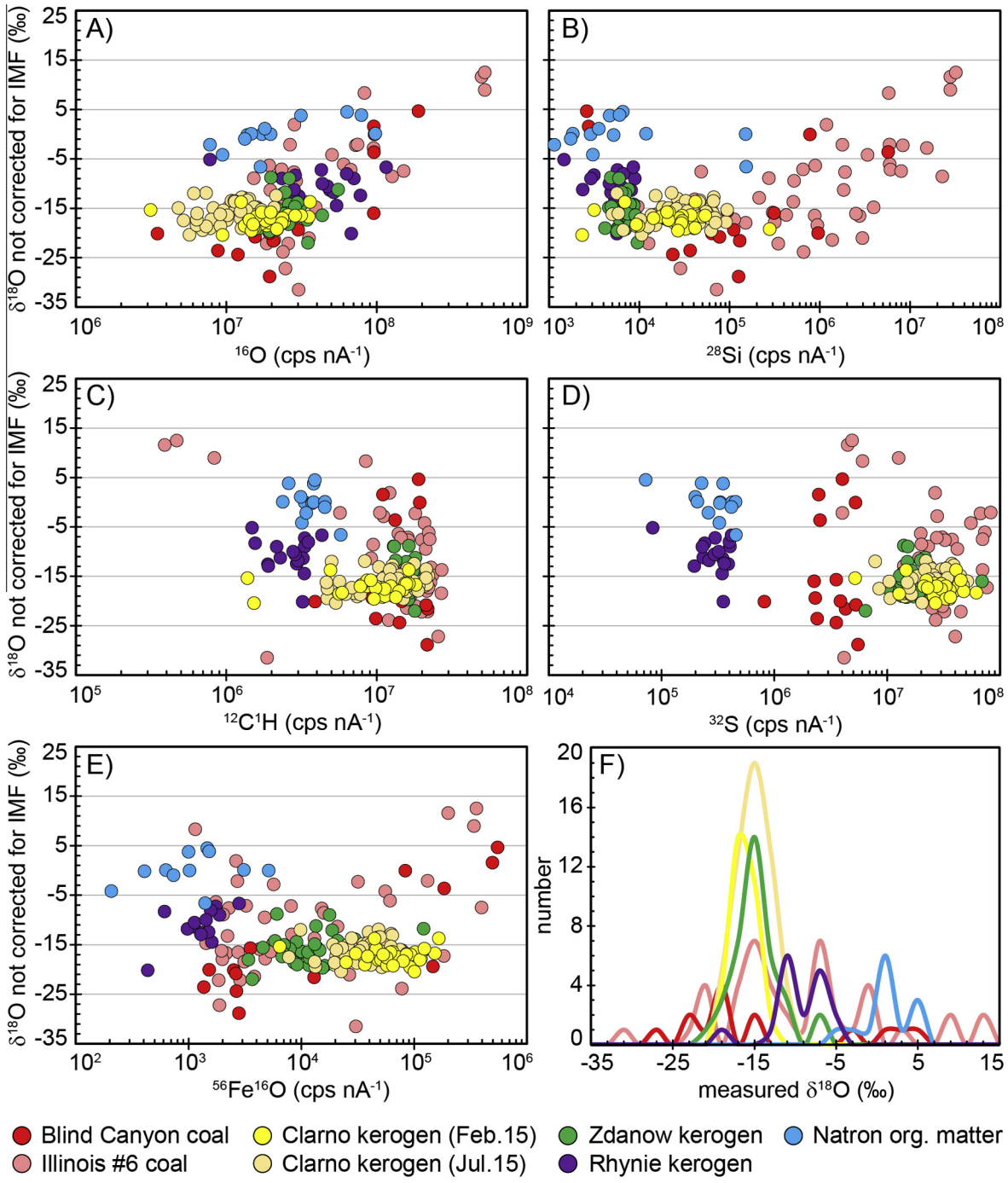

Fig. 2. Relative variations of the measured oxygen isotopic compositions, given as $\delta^{18}O$ values not corrected for IMF, versus ^{16}O (A), ^{28}Si (B), $^{12}C^{1}H$ (C), ^{32}S (D) and $^{56}Fe^{16}O$ (E) intensities. The distribution of the $\delta^{18}O$ values for each sample is also displayed as cumulative probability curves (F).

(Fig. 2). These measured intensities cannot be directly converted into C (or O, Si, etc.) contents because all the individual analyses are characterised by variable topography and surface flatness, since the OM powders were pressed into indium. However, on average these intensities are related to the bulk composition of the samples. This can be verified for $^{12}C^{1}H$ intensities, for example, which are consistent with the bulk C contents (Table 2) for both the coals and kerogen samples: ~2–4 × 10^6 cps nA^{-1} for Rhynie (C_{bulk} ~ 31 wt.%), 0.5–2.0 × 10^7 cps nA^{-1} for Clarno (C_{bulk} ~ 45 wt.%), 1.0–2.0 × 10^7 cps nA^{-1} for Zdanow (C_{bulk} ~ 69 wt.%) and ~2.0–3.0 × 10^7 cps nA^{-1} for the coal samples, which have the highest bulk C contents around 80 wt.%. The Illinois #6 coal sample also displays ^{32}S intensities about one order of magnitude higher than those measured on the Blind Canyon coal sample (Fig. 2), which is

consistent with their bulk organic S contents of ~2.4 wt.% and ~0.4 wt.%, respectively (Vorres, 1990). Clarno and Zdanow kerogens contain amounts of S similar to those of the Illinois #6 coal, while the Rhynie kerogen and Natron OM are characterised by very low S contents (Fig. 2).

The O isotope compositions show complex relationships with the intensities measured for $^{12}C^{1}H$, ^{16}O, ^{28}Si, ^{32}S and $^{56}Fe^{16}O$ at the spot scale (Fig. 2). In the coal samples, the measured $\delta^{18}O$ values are correlated with ^{16}O intensities, and either with ^{28}Si or $^{56}Fe^{16}O$ intensities (Fig. 2). Finally, the $^{12}C^{1}H$, ^{16}O, ^{28}Si, ^{32}S and $^{56}Fe^{16}O$ intensities also show complex relationships with each other, with in most cases clear linear trends towards the diagrams' origin (Fig. 3), indicating the presence of variable amount of porosity in each individual analysis.

4.3. Mineral inclusions in coal samples and kerogen residues

As stated in Section 3.1, a potential issue associated with microbeam analysis of kerogen samples is related to the presence of micro-inclusions of various mineral phases, not totally dissolved during the HF-HCl digestion of the chert samples. The effect of such inclusions is naturally stronger for the coal samples, which have not undergone any HF-HCl treatment, and which show ^{28}Si intensities one to two order of magnitude higher than kerogen samples (Fig. 3), indicating the presence of many silicate micro-inclusions. We have developed an approach that allows to identify and quantify the inclusions by monitoring the $^{12}C^{1}H$, ^{16}O, ^{28}Si, ^{32}S and $^{56}Fe^{16}O$ signals in the spot locations where O isotope analyses were carried out, which proved to be an effective way to identify contamination by such micro-inclusions during SIMS analysis of OM samples. Fig. 4 shows, for example, that SEM imaging of SIMS spots (Fig. 4A–C) characterised by anomalously high ^{28}Si, ^{32}S and/or $^{56}Fe^{16}O$ (Fig. 4D) indeed revealed the presence of mineral micro-inclusions, such as of silica, sulphides and/or Cr-rich minerals based on EDS analysis (Fig. 4E).

5. DISCUSSION

5.1. Treatment of the measured $^{18}O/^{16}O$ ratios to account for the presence of mineral inclusions

The large range of oxygen isotope variations observed in individual samples at the scale of tens of microns likely result from (i) the heterogeneity of OM, (ii) the presence of various mineral inclusions under the ion probe beam and (iii) the samples' topography, which is inherent to the pressing of OM powders into indium. The effect of topography on the analysis of homogeneous OM should

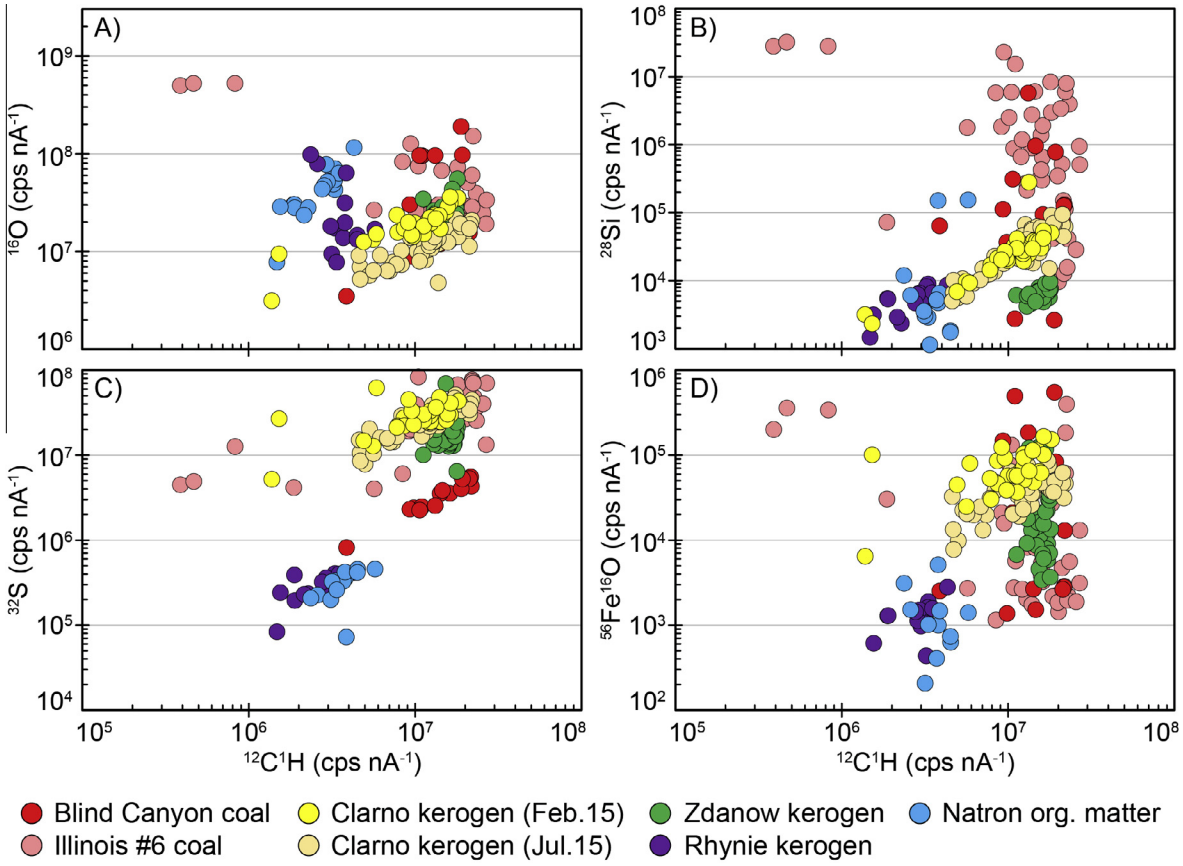

Fig. 3. Measured ^{16}O (A), ^{28}Si (B), ^{32}S (C) and $^{56}Fe^{16}O$ (D) secondary intensities (normalised to the primary beam intensity) versus $^{12}C^{1}H$ secondary intensity.

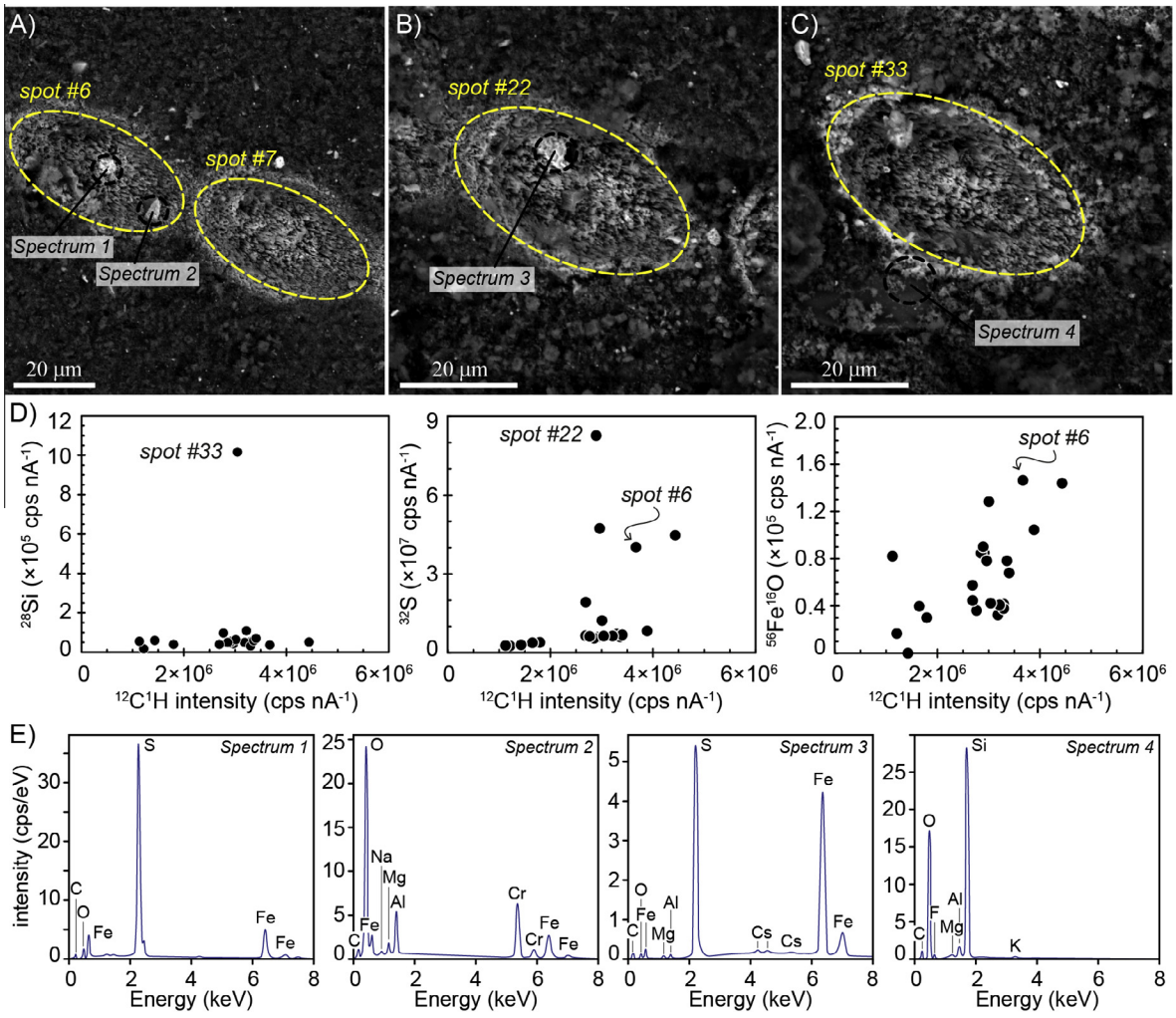

Fig. 4. (A-C) Back-scattered electron images of selected ion probe spots in a kerogen residue containing mineral micro-inclusions. (D) ^{28}Si, ^{32}S and $^{56}Fe^{16}O$ versus $^{12}C^{1}H$ intensities measured for all the analyses carried out on this kerogen sample. (E) EDS spectra of micro-inclusions found in analytical spots #6, #22 and #33, corresponding to sulphides, quartz and a Cr-rich mineral.

theoretically result in inter-element mixing trends pointing to the origin, as shown to various degrees by all the samples (Fig. 3). Outliers to such trends reflect the presence of mineral inclusions in the corresponding spots. A procedure was developed to exclude all measurements affected by the presence of mineral inclusions from the data set. In binary diagrams of ^{28}Si, ^{32}S and $^{56}Fe^{16}O$ versus $^{12}C^{1}H$, linear regressions passing through the origin were calculated, together with their 5σ confidence intervals (such an interval ensures that only true outliers are discarded, and not analyses resulting from the variability of OM). Outliers falling outside these intervals were interpreted as analyses contaminated by the presence of micro-mineral inclusions during sputtering, and were discarded. This is illustrated in Fig. 5 for measurements carried out during the February 2015 analytical session on the Clarno kerogen: a total of 8 spots can be discarded on the basis of anomalously high ^{28}Si (1 spot excluded; Fig. 5A), ^{32}S (4 spots excluded; Fig. 5B) and $^{56}Fe^{16}O$ (6 spots excluded; Fig. 5C). The extreme ranges of ^{28}Si intensities measured in the coal samples (Fig. 3) forced us to first pre-filter the data visually by excluding analyses corresponding to ^{28}Si intensities above 3×10^5 and 1×10^7 for Blind Canyon and Illinois #6, respectively, before applying the screening procedure detailed above.

The presence of sub-micron size silicate and oxide inclusions in such spots with anomalously high Si, S and Fe intensities has necessarily contaminated the O signal emitted from the OM since they have a higher O emissivity than OM. For example, we measured a ^{18}O emissivity of ~3–5 cps ppm^{-1} O nA^{-1} for the CRPG reference quartz NL615, compared to a ^{18}O emissivity of ~0.4–0.5 cps ppm^{-1} O nA^{-1} for the coal samples FOUT and AMB studied by Sangély et al. (2005). Similarly, magnetite analysed using a similar protocol with the Cameca 1280 ion microprobe at the University of Wisconsin yielded an emissivity for ^{18}O of ~10 cps ppm^{-1} O nA^{-1} (Huberty et al., 2010).

Screening the data to exclude analyses contaminated by O emitted by mineral inclusions greatly reduces the range measured for $\delta^{18}O$ values, especially for the two coal samples that did not underwent the acid maceration procedure. However, most of the kerogen samples still display a

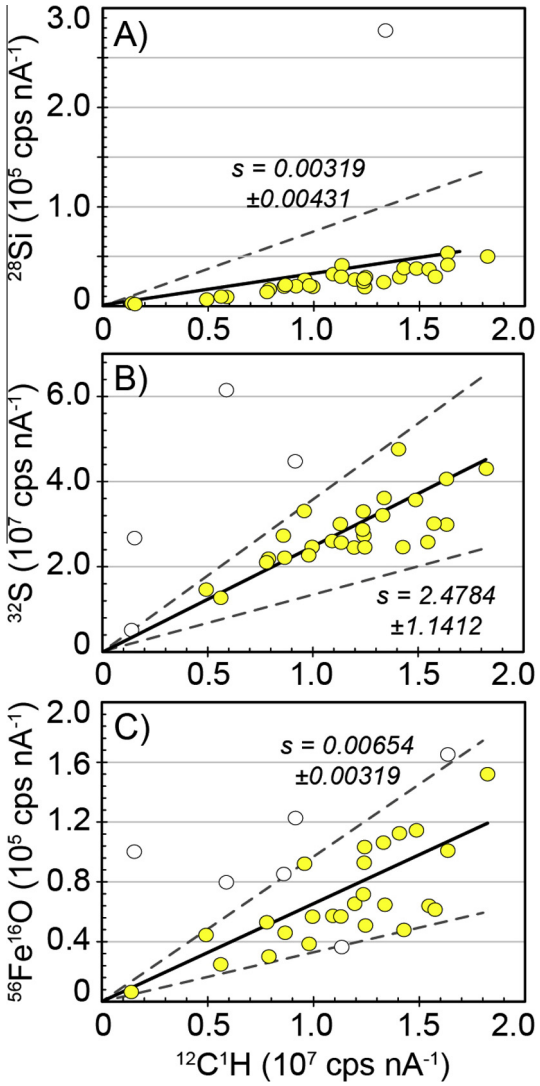

Fig. 5. Measured ^{28}Si (A), ^{32}S (B) and ^{56}Fe^{16}O (C) secondary intensities versus ^{12}C^{1}H intensity for analyses carried out on the Clarno kerogen in February 2015, illustrating how data can be filtered to exclude analyses compromised by O emitted from micro-inclusions of residual silicates, oxides and sulphides. The slopes of the regressions passing through the origin (*s*) are reported together with their 5σ confidence intervals (dotted grey lines), and data falling outside these intervals (empty circles) were considered as outliers (see text for details).

significant range (about 5–10‰, and up to ~20‰ for the Illinois coal sample, see below) of $\delta^{18}O$ values (Fig. 6), which is likely related to the OM structural and compositional heterogeneous nature at the micro-scale.

5.2. Validation of a standard for determining the instrumental mass fractionation during ion probe analysis of OM oxygen isotope composition

Homogeneity is one of the key characteristics required for a material to be used as a standard for micro-analytical techniques. Among the studied samples, the Clarno kerogen is the most homogeneous in terms of $\delta^{18}O$ values, yielding average $\delta^{18}O$ values (not corrected for IMF) of -17.3 ± 0.5‰ (2SE, $n = 23$) for the February 2015 session and -16.3 ± 0.9‰ (2SE, $n = 20$) for the July 2015 session. Therefore, the Clarno kerogen ($\delta^{18}O_{bulk} = 14.3 \pm 0.1$‰) was used as an internal reference material to determine instrumental mass fractionation (IMF, defined as $[1000 \times (^{18}O/^{16}O_{measured}/^{18}O/^{16}O_{true} - 1)]$) taking place during ion probe measurements of OM oxygen isotope composition (small quantities of this kerogen are available upon request). Values for IMF of -31.2 ± 0.5‰ are obtained for the February 2015 session using the 1280 HR ion probe, and of -30.2 ± 0.9‰ for the July 2015 session using the 1270 E7 ion probe. All the $\delta^{18}O$ data given in Supplementary Table 2 have been corrected using these IMF values, and their associated 2σ uncertainties include the error introduced by this correction.

In a detailed study of parameters influencing SIMS measurement of the C isotope composition in OM, Sangély et al. (2005) have shown that the atomic H/C ratio of the OM has a strong effect on the measured C isotope composition, with variations of up to ~5‰ for H/C ratios ranging from around 0 to ~1.7. In this study, only one kerogen sample is homogeneous enough to be used as an internal OM standard, and, therefore, we cannot precisely evaluate the role of varying H/C ratios on the measured O isotope compositions. However, the range of H/C ratios for the studied OM samples is relatively restricted, between 0.45 and 0.86 (Table 2). For such a range, the variations of IMF for C isotope compositions are within about 1‰ (Sangély et al., 2005). Therefore, matrix effect-induced O isotope variations are likely not significant in the studied samples compared to all the other sources of uncertainty. Anyway, this will have to be thoroughly tested once a set of standard OM materials with a large range of H/C ratios will be available for oxygen isotope measurements.

5.3. $\delta^{18}O$ variability in the coal and kerogen samples

The present SIMS data on fossil OM show the systematic presence of several per mill variations of the oxygen isotopic composition both (i) at the micrometre-scale within a given sample and (ii) in bulk between different samples (Fig. 7). The Blind Canyon coal has $\delta^{18}O$ values ranging from about 2–15‰, with an average $\delta^{18}O$ of 8.7 ± 3.6‰ (2SE, $n = 6$) and a median $\delta^{18}O$ of 8.6‰ (Table 2 and Fig. 7). For the Illinois #6 coal, the $\delta^{18}O$ values range from ~4‰ to 33‰, with an average $\delta^{18}O$ of 16.6 ± 2.6‰ (2SE, $n = 24$), and a slightly lower median $\delta^{18}O$ of 15.1‰ (Table 2 and Fig. 7). The oxygen isotope compositions of the kerogen samples are more homogeneous with similar average and median $\delta^{18}O$ values for each sample (Table 2 and Fig. 7): $\delta^{18}O$ values from ~12‰ to 18‰ for the Clarno kerogen, with an average $\delta^{18}O$ value of 13.9 ± 0.5‰ (2SE and $n = 43$; median $\delta^{18}O = 14.0$‰), from ~12‰ to 23‰ for the Zdanow kerogen, with an average $\delta^{18}O$ value of 15.3 ± 1.2‰ (2SE and $n = 19$; median $^{18}O = 14.8$‰), from ~10‰ to 22‰ for the Rhynie kerogen, with an average $\delta^{18}O$ value of 19.0 ± 2.1‰ (2SE and $n = 12$; median $\delta^{18}O = 19.3$‰), and from ~26‰ to 34‰ for the Natron OM, with an average $\delta^{18}O$ value of 30.3 ± 1.7‰ (2SE,

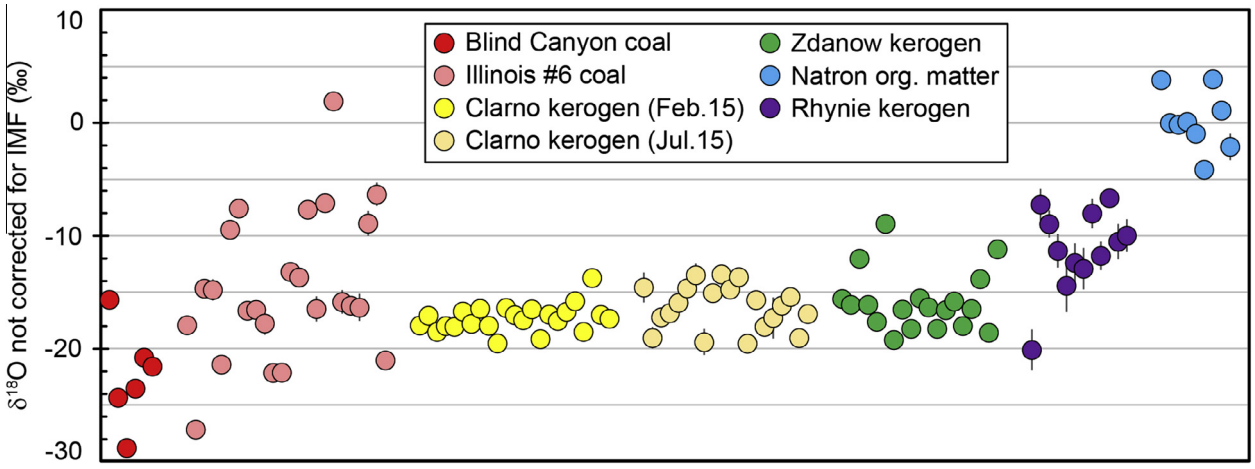

Fig. 6. Oxygen isotopic compositions (given as $\delta^{18}O$ values not corrected for instrumental mass fractionation) measured by SIMS on the coal and kerogen samples (plotted according to their analysis number), after discarding spots compromised by the presence of mineral inclusions (see text). Error bars represent 2σ internal uncertainties.

$n = 9$). Fig. 7 shows that there is a good match between bulk $\delta^{18}O$ values measured by TC/EA-IRMS and average $\delta^{18}O$ values calculated from SIMS analyses. This observation indicates that these two techniques apparently measure the same O signals in OM, and cross-validates the two techniques at the same time. Additionally, the SIMS technique demonstrates the presence of a large $\delta^{18}O$ variability at the micrometre-scale, which is potentially an important parameter to constrain the origin and preservation of the oxygen isotopic signal in fossil OM.

5.4. O isotope signature preservation in OM over geological times

One of the apparent characteristics of the kerogen and coal samples revealed by SIMS analyses is the large spread of their $\delta^{18}O$ values. Such observation is not surprising. Indeed, large isotopic variations of ~5–10‰ around an average value consistent with bulk determinations have also been observed for *in situ* $\delta^{13}C$ values of individual microfossils in kerogen samples (e.g., House et al., 2000; Wacey et al., 2011; Williford et al., 2013). Similar observations have also been made for $\delta^{18}O$ values determined *in situ* in cherts themselves, ranging in age from Eocene to Palaeoproterozoic, indicating the absence of significant effects due to diagenetic and/or late hydrothermal fluids since this would tend to homogenise the O isotope compositions (Marin-Carbonne et al., 2012, 2014). It has been argued that the $\delta^{13}C$ values determined *in situ* on microfossils enclosed within cherts ranging in age from 0.8 to 3.4 Ga represented pristine biological signatures that were not significantly affected by post-deposition processes (House et al., 2000; Wacey et al., 2011; Williford et al., 2013). Organic precursors in the Eocene and Early Devonian Clarno and Rhynie cherts, which did not suffer metamorphism, and in the Silurian Zdanow chert, which only

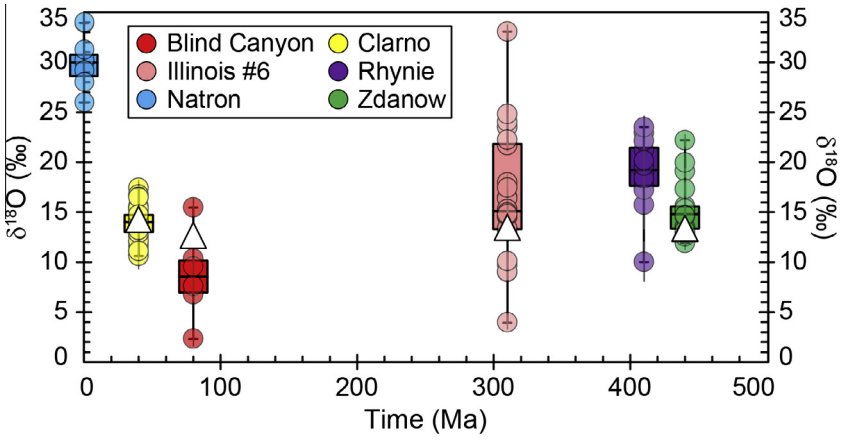

Fig. 7. SIMS $\delta^{18}O$ values corrected for IMF for the coal and kerogen samples versus sample ages. White triangles indicate the bulk $\delta^{18}O$ measured by TC/EA-IRMS, and black rectangles represent median $\delta^{18}O$ values calculated from SIMS analyses. Note the high $\delta^{18}O$ of Natron OM, which precipitated from hypersaline brines with elevated $\delta^{18}O$ values.

experienced prehnite-pumpellyite to pumpellyite-actinolite grade metamorphism, are well preserved (Bourbin, 2012; Bourbin et al., 2013). Therefore, it is likely that the $\delta^{18}O$ values measured on the Clarno, Rhynie and Zdanow kerogen samples were not affected by post-depositional processes, representing, therefore, the pristine biological O isotope signatures.

The coal samples were not protected within resistant silicified host rocks contrary to the kerogens. Nothing is known regarding effects of diagenesis and thermal maturation on the O isotope signatures of buried OM. On the other hand, it has been shown that thermal maturation can alter indigenous δD values, since an enrichment of D in hydrocarbon fractions and individual hydrocarbons is observed with increasing maturity (e.g., Dawson et al., 2005, 2007; Radke et al., 2005; Schimmelmann et al., 1999, 2006). Yet detailed studies have also shown that H isotope signatures can be preserved in immature sedimentary OM over hundreds of million years. For example, Dawson et al., 2004 have shown that *n*-alkanes from low-maturity Carboniferous and Permian torbanites (organic matter-rich sediments) preserve δD values that correlate with the paleoclimate at the time of the OM deposition. Similarly, Pedentchouk et al. (2006) found very little change in *n*-alkane δD values for maturities up to R_o of 0.7%, and argued that the preservation of subtle δD differences between compounds found in successive horizons suggests little exchange of hydrogen. Finally, Tuo et al. (2006) analysed D/H ratios in hydrocarbons of Eocene coal samples with maturation degrees similar to those of the Blind Canyon and Illinois #6 coal samples ($R_o \sim 0.5\%$) and argued that their indigenous H isotopic signatures remained largely preserved during diagenesis and the onset of OM maturation. If isotopic signatures of H, a very mobile element, in hydrocarbons in immature coal samples are not affected by diagenesis, it is likely that their O isotope signatures also remained pristine. Therefore, the $\delta^{18}O$ values measured in the immature Blind Canyon and Illinois #6 coal samples most likely correspond to those of the OM from which these coals formed.

5.5. From OM samples O isotope composition to water O isotope composition

Coal and kerogen samples are a mixture of heterogeneous components and are, therefore, particularly difficult to characterise, notably those formed in Phanerozoic continental environments. Elemental abundances of C, H, O, N, and S provide a first order indication regarding their composition, which reflects both their origin, but also the degree of thermal maturation as the latter induces progressive losses of H, N, O, and S relative to C through thermal aromatisation (e.g., Vandenbroucke and Largeau, 2007; Summons and Hallman, 2014). In addition, synchrotron-based *in situ* techniques, such as scanning transmission X-ray microscopy coupled with near-edge X-ray absorption fine structure, provide information on the types of C-containing functional groups (e.g., aromatic, aliphatic, carboxylic, alcoholic) in organic matter samples (e.g., Bernard et al., 2009, and references therein). In a pioneer study, Dunbar and Wilson (1983) analysed the bulk O isotope composition of low rank coal, lignite and peat samples from New Zealand, compared it with that of various coal precursors such as cellulose, lignin and resins, and argued that the major source of O in coal was cellulose. However, the $\delta^{18}O$ values measured on low rank coal, lignite and peat samples ($\delta^{18}O \sim 19$–$21‰$) were distinctly lower than the $\delta^{18}O_{cellulose}$ of ~27‰. Also, a fourth sample of higher rank coal yielded a $\delta^{18}O$ value of ~13‰, which is much more consistent with the $\delta^{18}O$ values measured by Dunbar and Wilson (1983) on a resin sample ($\delta^{18}O \sim 11‰$) and on lipids extracted from a peat sample ($\delta^{18}O \sim 13‰$). More recently, Silva et al. (2015) analysed the O isotope composition of cellulose samples of various C_3 and C_4 plant species and obtained $\delta^{18}O$ values of ~26–34‰, which is about $\sim 38 \pm 4‰$ higher than the average annual meteoric water $\delta^{18}O$ value of −8‰. It is commonly assumed that $\delta^{18}O_{cellulose}$ is elevated by $\sim 27 \pm 4‰$ compared to the $\delta^{18}O$ of the leaf water present during its synthesis (Epstein et al., 1977; DeNiro and Epstein, 1981; Cooper and DeNiro, 1989; Sternberg, 2009), suggesting that about 10‰ fractionation occurs during water transport from the roots to the leaves of the plants. Silva et al. (2015) also analysed the O isotope composition of the lipid fractions of the same plants and obtained $\delta^{18}O$ values of ~13–17‰, about $\sim 23 \pm 2‰$ above the average annual meteoric water $\delta^{18}O$ value. Cellulose quickly degrades during thermal maturation of plant biomass, in contrast to plant lipids that can persist in sediments due to their low biodegradability (Matsumoto et al., 2007) and be transformed into insoluble kerogens at moderate temperatures around 200–300 °C upon burial (Shioya and Ishiwatari, 1983). Therefore, the average O isotope compositions of the coal and kerogen samples analysed here should be compared with typical lipid O isotope compositions rather than with those of cellulose fractions.

The kerogen extracted from the Eocene Clarno chert mostly comprises remnants of continental plants (ferns, angiosperms, bryophytes) that composed flora of a marsh environment developed ~40 Myr ago in Oregon in the Western US. Based on detailed isotopic studies carried out on limestone and chert samples from the same age and the same region, it has been proposed that meteoric water precipitation in that area around 40 Ma was characterised by $\delta^{18}O$ values around −14‰ (Horton et al., 2004; Abruzzese et al., 2005). Waters in marsh environments typically experience intense evaporation processes, and are often characterised by $\delta^{18}O$ values ~6–10‰ higher compared with local meteoric waters (e.g., Monjerezi et al., 2011; Alvarez et al., 2015). Therefore, we postulate here that waters in which the Clarno flora lived were characterised by $\delta^{18}O$ values of around $-6 \pm 2‰$. Based on this water O isotope composition and using the average SIMS $\delta^{18}O$ signatures measured in Clarno kerogen, we can calculate a value for $\Delta^{18}O_{kerogen\text{-}water}$ of $19.9 \pm 2.1‰$. Such a value is consistent with the $\Delta^{18}O_{lipid\text{-}water}$ obtained by Silva et al. (2015). Although different in nature, floras at the origin of the Rhynie kerogen and the Blind Canyon and Illinois #6 coal samples likely flourished in similar quiet, swampy and marshy environments. Using the

$\Delta^{18}O_{kerogen\text{-}water}$ value determined based on the Clarno kerogen, $\delta^{18}O$ values of -11.2 ± 4.1‰, -3.3 ± 3.3‰ and -0.9 ± 2.9‰ can be determined for waters coeval with OM at the origin of the Blind Canyon, Illinois #6 and Rhynie samples, respectively. Such a range for $\delta^{18}O_{water}$ is within the range of present-day continental waters ($\delta^{18}O$ values range between around 5‰ and −20‰, based on the composition of 8939 surface water samples collected between 1990 and 2015 compiled in the IAEA Global Network of Isotopes in Rivers database, https://nucleus.iaea.org/wiser/gnir.php). While these estimates are associated with a few per mill uncertainties, it is interesting to note that there seems to be a correlation between these $\delta^{18}O_{water}$ estimates and the rough latitude of the palaeo-environments from which these samples originate, similarly to what is observed today for surface waters. The lowest $\delta^{18}O_{water}$ estimates are for the US Clarno and Blind Canyon samples that formed at a latitude of around 40–45°N (Scotese et al., 1988), where present-day surface waters have $\delta^{18}O$ values clustering around −10‰. At variance, the Illinois #6 and Rhynie samples formed at latitudes of around 0° and −20°S, respectively (Scotese and McKerrow, 1990), and their $\delta^{18}O_{water}$ appear slightly higher, in agreement with most present-day surface waters at these latitudes ($\delta^{18}O$ values from ~0 to around −5‰).

In contrast to the continental OM from the coals, Clarno and Rhynie samples, the OM extracted from the Natron and Zdanow cherts originate from marine microorganisms (i.e., cyanobacteria). If numerous studies have investigated the O isotope composition of carbonates associated with cyanobacteria in order to derive palaeo-climatic and palaeo-environmental information (e.g., Pentecost and Spiro, 1990; Andrews et al., 1993, 1997), we are not aware of any O isotope investigation of cyanobacteria organic tissues. A handful of studies have reported the O isotope composition of microbial cells and spores (e.g., Kreuzer-Martin and Jarman, 2007) and of chitinous invertebrate remains, such as chironomid larva head capsules (Wooller et al., 2004, 2008; Wang et al., 2009; Verbruggen et al., 2011), and showed that their O isotope signatures were strongly correlated with the $\delta^{18}O$ of the water in which they grew, ~70% of the total organic oxygen being derived from ambient water (Kreuzer-Martin and Jarman, 2007; Wang et al., 2009). The relationship between $\delta^{18}O_{OM}$ and $\delta^{18}O_{water}$ for both microbe spores and chironomid larva head capsules were consistent with each other, being approximately given by $\delta^{18}O_{OM} \sim 0.75\ (\pm 0.05) \times \delta^{18}O_{water} + 19.5\ (\pm 1.0)$, in other words $\delta^{18}O_{OM}$ is enriched by around 20‰ compared to ambient waters.

The OM extracted from the Natron chert sample mostly contains cyanobacteria remnants. According to Behr and Röhricht (2000), these cherts essentially formed by silicification of calcified cyanobacteria mats in very shallow water pools containing high salt and silica concentrations. The lakes Magadi and Natron are fed by hot springs characterised by $\delta^{18}O$ values around −4‰ to −1‰ (O'Neil and Hay, 1973; Hillaire-Marcel and Casanova, 1987). Intense evaporation results in increasing $\delta^{18}O$ values of the lakes' waters. Analyses of stromatolites around the Lake Natron yielded $\delta^{18}O$ values of ~33.5 ± 0.5‰ (Hillaire-Marcel and Casanova, 1987), corresponding to $\delta^{18}O_{water}$ values of ~4.0 ± 2.1‰ assuming calcite formed in equilibrium with water at 30 ± 10 °C. At present, $\delta^{18}O$ values of up to ~8–10‰ have been reported for present-day hypersaline brines (O'Neil and Hay, 1973; Hillaire-Marcel and Casanova, 1987), consistent with elevated $\delta^{18}O$ values of up to ~12‰ we obtained on similar hypersaline brines collected in 2012. At the time of silicification, the cyanobacteria colonies likely co-existed with such supersaturated hypersaline brines with extreme silica abundances (20–60 ppm SiO_2 and 50–100 ppm SiO_2 in streams and hot springs, respectively, and ~300–1500 ppm SiO_2 in waters and borehole brines of the Lake Magadi; Jones et al., 1977). Therefore, we assume that cyanobacteria in the Lake Natron co-existed with highly evaporated brine-type waters at the time of silicification. Considering a range of value for $\delta^{18}O_{water}$ between 8‰ and 12‰, and the average SIMS $\delta^{18}O$ value measured in Natron OM of 30.3 ± 1.7‰, yields $\Delta^{18}O_{OM\text{-}water}$ in a conservative range comprised between ~18 ± 2‰ and 22 ± 2‰. Interestingly, this range is consistent with the $\Delta^{18}O_{OM\text{-}water}$ determined from microbe spores and chironomid larva head capsules. A possible effect of temperature cannot be precisely assessed from this study and this likely adds a further ~1‰ uncertainty to the $\Delta^{18}O_{OM\text{-}water}$ estimated here for cyanobacteria. Using the range of $\Delta^{18}O_{OM\text{-}water}$ estimated using the Natron OM and the average SIMS $\delta^{18}O$ signatures of the Zdanow kerogen yields an estimate of −5 ± 4‰ for the corresponding $\delta^{18}O_{water}$, which is consistent with the O isotope composition of Early Silurian seawater around −5 ± 1‰ estimated by Veizer and Prokoph (2015) based on analysis of brachiopod carbonates.

6. CONCLUSION

In this study, we have demonstrated that the O isotope composition of organic matter, in the form of coal and kerogen samples, can be determined accurately at the sub-per mill level using secondary ion mass spectrometry. The $\delta^{18}O$ values determined by SIMS are on average consistent with the bulk $\delta^{18}O$ values determined by TC/EA-IRMS, but often display large (~5–10‰) spreads of $\delta^{18}O$ showing the presence and preservation of organic compounds with variable initial $\delta^{18}O$ values. Most of the $\delta^{18}O$ values obtained on two immature coal samples and two kerogen residues extracted from the Eocene Clarno and Early Devonian Rhynie continental chert samples range between ~8‰ and ~22–24‰. Average $\delta^{18}O$ values of these samples yield estimates for coeval $\delta^{18}O_{water}$ from around −11‰ to −1‰, which are within the range of present-day continental waters. Analyses of cyanobacteria remnants from the Silurian Zdanow chert sample yielded $\delta^{18}O$ values in the range 12–20‰. Based on the O isotope composition measured on recent fossil cyanobacteria from the hypersaline Lake Natron in Tanzania, and on the O isotope composition of the lake waters in which they lived, we argue that $\delta^{18}O$ values of cyanobacteria remnants are enriched by about ~18 ± 2‰ to 22 ± 2‰ compared to coeval water. This relationship suggests that deep ocean waters in which the Zdanow cyanobacteria lived during Early Silurian times were characterised by $\delta^{18}O$ values of around −5 ± 4‰. In this study

we have focussed on Phanerozoic remnants of organic matter samples, derived from both continental and marine environments. Future studies notably targeting O isotope measurements of early-life remnants found as kerogens preserved in Archean cherts have the potential to provide crucial clues regarding the O isotopic composition of Archean oceans. Ultimately, combining these new constraints with the Archean chert O isotope record would allow reconstructing the temperature of oceans on the Early Earth.

ACKNOWLEDGMENTS

This research is supported by the ERC Grant No. 290861 – PaleoNanoLife. We would like to thank S. Pont for his help with SEM analysis at the MNHN, M. Bourbin for extraction of some of the kerogen residues, and J. W. Schopf for providing us with the Clarno chert sample, S. M. Awramik for the Rhynie chert sample, B. Kremer for the Zdanow chert sample and A. Person for the Natron chert sample. The associate editor Alex Nemchin and two anonymous referees are also thanked for their insightful comments. This is IPGP contribution #3725, and CRPG contribution #2432.

APPENDIX A. SUPPLEMENTARY DATA

Supplementary data associated with this article can be found, in the online version, at http://dx.doi.org/10.1016/j.gca.2016.02.035.

REFERENCES

Abruzzese M. J., Waldbauer J. R. and Chamberlain C. P. (2005) Oxygen and hydrogen isotope ratios in freshwater chert as indicators of ancient climate and hydrologic regime. *Geochim. Cosmochim. Acta* **69**, 1377–1390.

Alvarez M., Carol E. and Dapeña C. (2015) The role of evapotranspiration in the groundwater hydrochemistry of an arid coastal wetland (Península Valdés, Argentina). *Sci. Total Environ.* **506–507**, 299–307.

Andrews J. E., Riding R. and Dennis P. F. (1993) Stable isotopic compositions of recent freshwater cyanobacterial carbonates from the British Isles: local and regional environmental controls. *Sedimentology* **40**, 303–314.

Andrews J. E., Riding R. and Dennis P. F. (1997) The stable isotope record of environmental and climatic signals in modern terrestrial microbial carbonates from Europe. *Palaeogeogr. Palaeoclimatol.* **129**, 171–189.

Arnold C. A. and Daugherty L. H. (1964) A fossil Dennstaedtioid fern from the Eocene Clarno Formation of Oregon. *Contrib. Mus. Paleontolo. Univ. Michigan* **19**, 65–88.

Behr H. J. and Röhricht C. (2000) Record of seismotectonic events in siliceous cyanobacterial sediments (Magadi cherts), Lake Magadi, Kenya. *Int. J. Earth Sci.* **89**, 268–283.

Bernard S., Benzerara K., Beyssac O., Brown, Jr., G. E., Grauvogel Stamm L. and Duringer P. (2009) Ultrastructural and chemical study of modern and fossil sporoderms by scanning transmission X-ray microscopy (STXM). *Rev. Palaeobot. Palynol.* **156**, 248–261.

Bontognali T. R. R., Sessions A. L., Allwood A. C., Fischer W. W., Grotzinger J. P., Summons R. E. and Eiler J. M. (2012) Sulfur isotopes of organic matter preserved in 3.45-billion-year-old stromatolites reveal microbial metabolism. *Proc. Natl. Acad. Sci.* **109**, 15146–15151.

Bourbin M. (2012) Carbonaceous Matter in Archean Siliceous Sedimentary Rocks: from the Origins of Life on Earth to Exobiological Perspectives. Ph. D. thesis, University Paris Diderot, 143 p.

Bourbin M., Gourier D., Derenne S., Binet L., Le Du Y., Westall F., Kremer B. and Gautret P. (2013) Dating carbonaceous matter in Archean cherts by electron paramagnetic resonance. *Astrobiology* **13**, 151–162.

Brasier M. D., Antcliffe J., Saunders M. and Wacey D. (2015) Changing the picture of Earth's earliest fossils (3.5–1.9 Ga) with new approaches and new discoveries. *Proc. Natl. Acad. Sci. U. S. A.* **112**, 4859–4864.

Charnay B., Forget F., Wordsworth R., Leconte J., Millour E., Codron F. and Spiga A. (2013) Exploring the faint young Sun problem and the possible climates of the Archean Earth with a 3D GCM. *J. Geophys. Res. Atmos.* **118**, 10414–10431.

Cloutis E. A. (2003) Quantitative characterization of coal properties using bidirectional diffuse reflectance spectroscopy. *Fuel* **82**, 2239–2254.

Cooper L. and DeNiro M. (1989) Oxygen-18 content of atmospheric oxygen does not affect the oxygen isotope relationship between environmental water and cellulose in a submerged aquatic plant, *Egeria densa* Planch. *Plant Physiol.* **91**, 536–541.

Czaja A. D., Kudryavtsev A. B., Cody G. D. and Schopf J. W. (2009) Characterization of permineralized kerogen from an Eocene fossil fern. *Org. Geochem.* **40**, 353–364.

Dawson D., Grice K., Wang S. X., Alexander R. and Radke J. (2004) Stable hydrogen isotopic composition of hydrocarbons in torbanites (Late Carboniferous to Late Permian) deposited under various climatic conditions. *Org. Geochem.* **35**, 189–197.

Dawson D., Grice K. and Alexander R. (2005) Effect of maturation on the indigenous δD signatures of individual hydrocarbons in sediments and crude oils from the Perth Basin (Western Australia). *Org. Geochem.* **36**, 95–104.

Dawson D., Grice K., Alexander R. and Edwards D. (2007) The effect of source and maturity on the stable isotopic compositions of individual hydrocarbons in sediments and crude oils from the Vulcan Sub-basin, Timor Sea, Northern Australia. *Org. Geochem.* **38**, 1015–1038.

DeNiro M. J. and Epstein S. (1981) Isotopic composition of cellulose from aquatic organisms. *Geochim. Cosmochim. Acta* **45**, 1885–1894.

DiMichele W. A. and Phillips T. L. (1988) Paleoecology of the middle Pennsylvanian-age Herrin coal swamp (Illinois) near a contemporaneous river system, the Walshville paleochannel. *Rev. Palaeobot. Palynol.* **56**, 151–176.

Dunbar J. and Wilson A. T. (1983) The use of $^{18}O/^{16}O$ ratios to study the formation and chemical origin of coal. *Geochim. Cosmochim. Acta* **47**, 1541–1543.

Durand B. and Monin J. C. (1980) Elemental analysis of kerogens (C, H, O, N, S, Fe). In *Kerogen – Insoluble organic matter from sedimentary rocks* (ed. B. Durand). Technip, Paris, France, pp. 113–142.

Durand B. and Nicaise G. (1980) Procedures for kerogen isolation. In *Kerogen – Insoluble organic matter from sedimentary rocks* (ed. B. Durand). Technip, Paris, France, pp. 35–54.

Epstein S., Thompson P. and Yapp C. J. (1977) Oxygen and hydrogen isotopic ratios in plant cellulose. *Science* **198**, 1209–1215.

Eugster H. P. (1967) Hydrous sodium silicates from Lake Magadi, Kenya: precursors of bedded chert. *Science* **157**, 1177–1180.

Eugster H. P. (1969) Inorganic bedded cherts from the Magadi area, Kenya. *Contrib. Mineral. Petrol.* **22**, 1–31.

Evans D. A., Beukes N. J. and Kirschvink J. L. (1997) Low-latitude glaciation in the palaeoproterozoic era. *Nature* **386**, 262–266.

Fischer W. W., Fike D. A., Johnson J. E., Raub T. D., Guan Y., Kirschvink J. L. and Eiler J. M. (2014) SQUID–SIMS is a useful approach to uncover primary signals in the Archean sulfur cycle. *Proc. Natl. Acad. Sci.* **111**, 5468–5473.

Hay R. L. (1968) Chert and its sodium silicate precursors in sodium carbonate lakes of East Africa. *Contrib. Mineral. Petrol.* **17**, 255–274.

Hillaire-Marcel C. and Casanova J. (1987) Isotopic hydrology and paleohydrology of the Magadi (Kenya)-Natron (Tanzania) basin during the Late Quaternary. *Palaeogeogr. Palaeoclimatol.* **58**, 155–181.

Hillaire-Marcel C., Carro O. and Casanova J. (1986) ^{14}C and Th/U dating of Pleistocene and Holocene stromatolites from East African paleolakes. *Quat. Res.* **25**, 312–329.

Horton T. W., Sjostrom D. J., Abruzzese M. J., Poage M. A., Waldbauer J. R., Hren M., Wooden J. and Chamberlain C. P. (2004) Spatial and temporal variation of cenozoic surface elevation in the Great Basin and Sierra Nevada. *Am. J. Sci.* **304**, 862–888.

House C. H., Schopf J. W., McKeegan K. D., Coath C. D., Harrison T. M. and Stetter K. O. (2000) Carbon isotopic composition of individual Precambrian microfossils. *Geology* **28**, 707–710.

Hren M. T., Tice M. M. and Chamberlain C. P. (2009) Oxygen and hydrogen isotope evidence for a temperate climate 3.42 billion years ago. *Nature* **462**, 205–208.

Huberty J. M., Kita N. T., Kozdon R., Heck P. R., Fournelle J. H., Spicuzza M. J., Xu H. and Valley J. W. (2010) Crystal orientation effects in δ^{18}O for magnetite and hematite by SIMS. *Chem. Geol.* **276**, 269–283.

Jaffrés J. B. D., Shields G. A. and Wallmann K. (2007) The oxygen isotope evolution of seawater: a critical review of a long-standing controversy and an improved geological water cycle model for the past 3.4 billion years. *Earth Sci. Rev.* **83**, 83–122.

Jones B. F., Eugster H. P. and Rettig S. L. (1977) Hydrochemistry of the Lake Magadi basin, Kenya. *Geochim. Cosmochim. Acta* **41**, 53–72.

Kasting J. F., Howard M. T., Wallmann K., Veizer J., Shields G. and Jaffres J. (2006) Paleoclimates, ocean depth, and the oxygen isotopic composition of seawater. *Earth Planet. Sci. Lett.* **252**, 82–93.

Knauth L. P. (2005) Temperature and salinity history of the Precambrian ocean: implications for the course of microbial evolution. *Palaeogeogr. Palaeoclimatol.* **219**, 53–69.

Knauth L. P. and Epstein S. (1976) Hydrogen and oxygen isotope ratios in nodular and bedded cherts. *Geochim. Cosmochim. Acta* **40**, 1095–1108.

Knauth L. P. and Lowe D. R. (1978) Oxygen isotope geochemistry of cherts from Onverwacht group (3.4 Billion Years), Transvaal, South-Africa, with implications for secular variations in isotopic composition of cherts. *Earth Planet. Sci. Lett.* **41**, 209–222.

Knauth L. P. and Lowe D. R. (2003) High Archean climatic temperature inferred from oxygen isotope geochemistry of cherts in the 3.5 Ga Swaziland Supergroup, South Africa. *Geol. Soc. Am. Bull.* **115**, 566–580.

Kremer B. (2006) Mat-forming coccoid cyanobacteria from early Silurian marine deposits of Sudetes, Poland. *Acta Palaeontol. Pol.* **51**, 143–154.

Kremer B. and Kaźmierczak J. (2005) Cyanobacterial mats from Silurian black Radiolarian cherts: phototrophic life at the edge of darkness? *J. Sediment. Res.* **75**, 895–904.

Kreuzer-Martin H. W. and Jarman K. H. (2007) Stable isotope ratios and forensic analysis of microorganisms. *Appl. Environ. Microb.* **73**, 3896–3908.

Lowe D. R. and Tice M. M. (2004) Geologic evidence for Archean atmospheric and climatic evolution: fluctuating levels of CO_2, CH_4, and O_2 with an overriding tectonic control. *Geology* **32**, 493–496.

Marin J., Chaussidon M. and Robert F. (2010) Microscale oxygen isotope variations in 1.9 Ga Gunflint cherts: assessments of diagenesis effects and implications for oceanic paleotemperature reconstructions. *Geochim. Cosmochim. Acta* **74**, 116–130.

Marin-Carbonne J., Chaussidon M. and Robert F. (2012) Micrometer-scale chemical and isotopic criteria (O and Si) on the origin and history of Precambrian cherts: implications for paleo-temperature reconstructions. *Geochim. Cosmochim. Acta* **92**, 129–147.

Marin-Carbonne J., Chaussidon M. and Robert F. (2014) The silicon and oxygen isotope compositions of Precambrian cherts: a record of oceanic paleo-temperatures? *Precamb. Res.* **247**, 223–234.

Mark D. F., Rice C. M., Fallick A. E., Trewin N. H., Lee M. R., Boyce A. and Lee J. K. W. (2011) ^{40}Ar/^{39}Ar dating of hydrothermal activity, biota and gold mineralization in the Rhynie hot-spring system, Aberdeenshire, Scotland. *Geochim. Cosmochim. Acta* **75**, 555–569.

Matsumoto K., Kawamura K., Uchida M. and Shibata Y. (2007) Radiocarbon content and stable carbon isotopic ratios of individual fatty acids in subsurface soil: implication for selective microbial degradation and modification of soil organic matter. *Geochem. J.* **41**, 483–492.

Monjerezi M., Vogt R. D., Aagaard P., Gebru A. G. and Saka J. D. (2011) Using ^{87}Sr/^{86}Sr, δ^{18}O and δ^{2}H isotopes along with major chemical composition to assess groundwater salinization in lower Shire valley, Malawi. *Appl. Geochem.* **26**, 2201–2214.

O'Neil J. R. and Hay R. L. (1973) ^{18}O/^{16}O ratios in cherts associated with the saline lake deposits of East Africa. *Earth Planet. Sci. Lett.* **19**, 257–266.

Parker L. R. (1976) Paleoecology of the fluvial coal-forming swamps and associated floodplain environments in the Blackhawk Formation of central Utah. *Brigham Young Univ. Geol. Stud.* **22**, 99–116.

Pedentchouk N., Freeman K. H. and Harris N. B. (2006) Different response of δD values of *n*-alkanes, isoprenoids and kerogen during thermal maturation. *Geochim. Cosmochim. Acta* **70**, 2063–2072.

Pentecost A. and Spiro B. (1990) Stable carbon and oxygen isotope composition of calcites associated with modern freshwater cyanobacteria and algae. *Geomicrobiol. J.* **8**, 17–26.

Perry, Jr., E. C. (1967) The oxygen isotopic chemistry of ancient cherts. *Earth Planet. Sci. Lett.* **3**, 62–66.

Perry Jr. E. C. and Lefticariu L. (2014) 9.5 – Formation and Geochemistry of Precambrian cherts. In *Treatise on Geochemistry* second ed. (eds. H. D. Holland and K. K. Turekian), Elsevier, Oxford. pp. 113–139.

Pierce B. S., Stanton R. W. and Cecil C. B. (1989) Coal quality characteristics of the Blind Canyon coal bed, Utah, source of the Argonne #6 premium sample. U.S. Geological Survey Professional Open-File Report 89–634, 28 p.

Pope E. C., Bird D. K. and Rosing M. T. (2012) Isotope composition and volume of Earth's early oceans. *Proc. Natl. Acad. Sci. U.S.A.* **109**, 4371–4376.

Radke J., Bechtel A., Gaupp R., Püttmann W., Schwark L., Sachse D. and Gleixner G. (2005) Correlation between hydrogen isotope ratios of lipid biomarkers and sediment maturity. *Geochim. Cosmochim. Acta* **69**, 5517–5530.

Rice C. M., Ashcroft W. A., Batten D. J., Boyce A. J., Caulfied J. B. D., Fallick A. E., Hole M. J., Jones E., Pearson M. J., Rogers G., Saxton J. M., Stuart F. M., Trewin N. H. and Turner G. (1995) A Devonian auriferous hot-spring system, Rhynie, Scotland. *J. Geol. Soc. Lond.* **152**, 229–250.

Rice C. M., Trewin N. H. and Anderson L. I. (2002) Geological setting of the Early Devonian Rhynie cherts, Aberdeenshire, Scotland: an early terrestrial hot spring system. *J. Geol. Soc. Lond.* **159**, 203–214.

Robert F. and Chaussidon M. (2006) A palaeo-temperature curve for the Precambrian oceans based on silicon isotopes in cherts. *Nature* **443**, 969–972.

Sangély L., Chaussidon M., Michels R. and Huault V. (2005) Microanalysis of carbon isotope composition in organic matter by secondary ion mass spectrometry. *Chem. Geol.* **223**, 179–195.

Schimmelmann A., Lewan M. D. and Wintsch R. P. (1999) D/H isotope ratios of kerogen, bitumen, oil, and water in hydrous pyrolysis of source rocks containing kerogen types I, II, IIS and III. *Geochim. Cosmochim. Acta* **63**, 3751–3766.

Schimmelmann A., Sessions A. L. and Mastalerz M. (2006) Hydrogen isotopic (D/H) composition of organic matter during diagenesis and thermal maturation. *Annu. Rev. Earth Planet. Sci.* **34**, 501–533.

Schopf J. W. (1993) Microfossils of the Early Archean Apex chert: new evidence of the antiquity of life. *Science* **260**, 640–646.

Schopf J. W., Hayes J. M. and Walter M. R. (1983) Evolution of Earth's earliest ecosystems: recent progress and unsolved problems. In *Earth's Earliest Biosphere* (ed. J. W. Schopf). Princeton Univ. Press, Princeton, New Jersey, pp. 361–384.

Scotese C. R. and McKerrow W. S. (1990) Revised World maps and introduction. In *Palaeozoic Palaeogeography and Biogeography* (eds. W. S. McKerrow and C. R. Scotese). Geol. Soc. Mem. 12, pp. 1–12.

Scotese C. R., Gahagan L. M. and Larson R. L. (1988) Plate reconstructions of the Cretaceous and Cenozoic ocean basins. *Tectonophysics* **155**, 27–48.

Shi C. S., Schopf J. W. and Kudryavtsev A. B. (2013) Characterization of the stem anatomy of the Eocene fern Dennstaedtiopsis aerenchymata (Dennstaedtiaceae) by use of confocal laser scanning microscopy. *Am. J. Bot.* **100**, 1626–1640.

Shioya M. and Ishiwatari R. (1983) Laboratory thermal conversion of sedimentary lipids to kerogen-like matter. *Org. Geochem.* **5**, 7–12.

Silva L. C. R., Pedroso G., Doane T. A., Mukome F. N. D. and Horwath W. R. (2015) Beyond the cellulose: oxygen isotope composition of plant lipids as a proxy for terrestrial water balance. *Geochem. Persp. Lett.* **1**, 33–42.

Sternberg L. (2009) Oxygen stable isotope ratios of tree-ring cellulose: the next phase of understanding. *New Phytol.* **181**, 553–562.

Sternberg L. and DeNiro M. J. D. (1983) Biogeochemical implications of the isotopic equilibrium fractionation factor between the oxygen atoms of acetone and water. *Geochim. Cosmochim. Acta* **47**, 2271–2274.

Summons R. E. and Hallman C. (2014) 12.2 – Organic geochemical signatures of early life on Earth. In *Treatise on Geochemistry* second ed. (eds. H. D. Holland and K. K. Turekian), Elsevier, Oxford. pp. 33–46.

Tice M. M. and Lowe D. R. (2004) Photosynthetic microbial mats in the 3,416-Myr-old ocean. *Nature* **431**, 549–552.

Tuo J., Zhang M., Wang X. and Zhang C. (2006) Hydrogen isotope ratios of aliphatic and diterpenoid hydrocarbons in coals and carbonaceous mudstones from the Liaohe Basin, China. *Org. Geochem.* **37**, 165–176.

Ueno Y., Isozaki Y., Yurimoto H. and Maruyama S. (2001) Carbon isotopic signatures of individual archean microfossils(?) from Western Australia. *Int. Geol. Rev.* **43**, 196–212.

Vandenbroucke M. and Largeau C. (2007) Kerogen origin, evolution and structure. *Org. Geochem.* **38**, 719–833.

Veizer J. and Prokoph A. (2015) Temperatures and oxygen isotopic composition of Phanerozoic oceans. *Earth Sci. Rev.* **146**, 92–104.

Verbruggen F., Heiri O., Reichart G. J., Blaga C. and Lottera A. F. (2011) Stable oxygen isotopes in chironomid and cladoceran remains as indicators for lake-water $\delta^{18}O$. *Limnol. Oceanogr.* **56**, 2071–2079.

Vorres K. S. (1990) The Argonne premium coal sample program. *Energy Fuel.* **4**, 420–426.

Wacey D., Kilburn M. R., Saunders M., Cliff J. and Brasier M. D. (2011) Microfossils of sulphur-metabolizing cells in 3.4-billion-year-old rocks of Western Australia. *Nat. Geosci.* **4**, 698–702.

Walter M. R., Hofmann H. J. and Schopf J. W. (1983) Geographic and geologic data for processed rock samples. In *Earth's Earliest Biosphere* (ed. J. W. Schopf). Princeton Univ. Press, Princeton, New Jersey, pp. 385–413.

Wang Y. V., O'Brien D. M., Jenson J., Francis D. and Wooller M. J. (2009) The influence of diet and water on the stable oxygen and hydrogen isotope composition of Chironomidae (Diptera) with paleoecological implications. *Oecologia* **160**, 225–233.

Williford K. H., Ushikubo T., Schopf J. W., Lepot K., Kitajima K. and Valley J. W. (2013) Preservation and detection of microstructural and taxonomic correlations in the carbon isotopic compositions of individual Precambrian microfossils. *Geochim. Cosmochim. Acta* **104**, 165–182.

Willman H. B., Atherton E., Buschbach T. C., Collinson C., Frye J. C., Hopkins M. E., Lineback J. A. and Simon J. A. (1975) Handbook of Illinois Stratigraphy. *Illinois State Geol. Surv. Bull.* 95, 261p.

Wooller M. J., Francis D., Fogel M. L., Miller G. H., Walker I. R. and Wolfe A. P. (2004) Quantitative paleotemperature estimates from $\delta^{18}O$ of chironomid head capsules preserved in Arctic lake sediments. *J. Paleolimnol.* **31**, 267–274.

Wooller M. J., Wang Y. and Axford Y. (2008) A multiple stable isotope record of Late Quaternary limnological changes and chironomid paleoecology from northeastern Iceland. *J. Paleolimnol.* **40**, 63–77.

Young G. M., Brunn V. V., Gold D. J. C. and Minter W. E. L. (1998) Earth's oldest reported glaciation: physical and chemical evidence from the Archean Mozaan group (2.9 Ga) of South Africa. *J. Geol.* **106**, 523–538.

Associate editor: Alexander Nemchin